Article

Effect of Scarf Repair Geometry on the Impact Performance of Aerospace Composites

Sridharan Vijay Shankar[1] and Sridhar Idapalapati[1,2,*]

[1]Rolls-Royce @ NTU Corporate Laboratory, Nanyang Technological University, Singapore 639798, Singapore

(Now with the School of Materials Science and Engineering) (Email: sridhara001@e.ntu.edu.sg)

[2]School of Mechanical and Aerospace Engineering, Nanyang Technological University, Singapore 639798, Singapore (Email: msridhar@ntu.edu.sg)

* Correspondence: msridhar@ntu.edu.sg

Abstract: This experimental study investigates the effect of scarf geometry in restoring the impact response of scarf patched 3 mm thick glass-fibre reinforced polymer (GFRP) matrix composite laminates. Traditional circular along with rounded rectangular scarf patch configurations considered as repair patches. Experimental measurements revealed that the temporal variations of force and energy response of the pristine specimen are close to that of circular repaired specimens. The predominant failure modes were witnessed only in repair patch which include the matrix cracking, fibre fracture, delamination and no discontinuity in adhesive interface was witnessed. When compared with the pristine samples, the top ply damage size of the of the circular repaired specimens is larger by 9.91 %, while that of the rounded rectangular repaired specimens is larger by 434.23 %. The results show that circular scarf repair is more suitable choice of repair approach under the condition of 37J low-velocity impact event even though the global force-time response is similar.

Keywords: Scarf patch; Film adhesive; Secondary bonding; Impact loading; Failure analysis

1. Introduction

The continual drive for re-engineering of glass fibre reinforced polymer (GFRP) based load bearing components have opened avenues for design for repair. Particularly, when load bearing composite components operate in diverse conditions, they are susceptible to foreign object impact during operational stage as well as accidental tool drop impacts during maintenance, repair and overhaul (MRO) events [1]. These accidents can induce barely visible damages to laminate delamination initiated by matrix cracking and its channelling through fibres or concentrated commuted fracture, consequently reducing laminate strength and stiffness [2]. Particularly, low-velocity impact damage includes different damage mechanisms such as delamination, matrix cracking, fibre failure and through penetration. Panettieri et al. [3] analyzed low energy impacts from 4.5J to 30J on quasi-isotropic carbon fiber reinforced polymer (CFRP) with different thicknesses. They pointed out that large contact force fluctuations due to delamination onset, but the subsequent ultrasonic scans did not reveal any significant internal damage. Mehmet et al. [4] investigated impact response of unidirectional GFRP and further discussed damage modes and damage processes based on variation of absorbed energy (E_a) and impact energy (E_i). They found that the primary damage mode for higher impact energies was found to be fiber fracture whereas, for smaller impact energies it was indentation resulting in delamination and matrix cracks. Koloor et.al. [5] found that delamination of laminas lowers flexural strength up to 46.7% compared to their pristine sample, when they are under transverse loading. Hall et. al. [6] found that the delaminations form between plies of different fibre orientations and tend to grow along the orientation of the ply beneath the delamination.

Selective parameters that influence the restoration of structural properties like includes impact energy, impact location within the repaired area, type of bond and shape of repair patch. Effect of impact energy and impact location on the size of the composite's damage area were extensively

Preprints (www.preprints.org) | NOT PEER-REVIEWED | Posted: 25 April 2023 doi:10.20944/preprints202304.0866.v1

studied in the past [7]. The patch shape can influence the reduction in the stress intensity factor and hence restoration of structural strength [8]. Mechanical fastening and adhesive bonding are the two main approaches used to repair damaged structures to restore them to ultimate design strength. For aircraft structures, adhesively bonded scarf joint is typically used, as it does not produce protrusions that disrupt the aerodynamic performance of the structure [9] and minimizes joint eccentricities. For identical adherends, scarf joints use relatively small scarf angles to transfer loads efficiently as it distributes shear stresses uniformly in the adhesive layer and low peel stresses at the joint interface and making them a viable MRO option for repairing composite structures [10]. Pengcheng et. al.[11] in their work demonstrated maximum tensile strength can be achieved if variation between the fiber orientations of patch and the laminate is zero. Similalrly, Gursahib et. al. [12] in their work determined that the repair of main load bearing plies (0°) of parent laminate with $[45]_2$ patches presented the most favourable residual tensile behaviour by effectively releasing the stress concentration in the damaged area.

Significant changes in tension, compression and impact properties have been observed across different scarf angles [13]. The analysis showed that the increase in scarf angle led to a decrease in tensile and compressive strength. Yet it is undesirable to decrease the scarf angle, as removing excessive material from the parent laminate can be detrimental to the restoration of structural properties [13]. In order to find the optimal design space for scarf angle, an equilibrium between laminate limiting strength to adhesive limiting strength must be determined [14].

Considering the relevance of composite scarf repair in the current aerospace and marine industry, it is necessary to adopt appropriate scarf patch shapes to restore the damaged structure. Popularly studied repair profiles like circular repair patches [8, 15, 16] have shown promises of reinstating the damaged structures but it also comes with a penalty of removing greater volume of undamaged regions which adds to the time penalty for the repair. In the past works on various repair shapes such as: elliptical [8, 16], square [8, 15], rhombus[15], oval [16] and hexagon [15, 16] were conducted. No experimental study has been performed to understand the influence of large sample size (250 mm side square) on low velocity impact and level of strength restoration when different scarf geometries with same patch repair volume. Therefore, in this experimental research, we investigate the impact response of 3mm thick GFRP laminates repaired by circular and rounded rectangular scarf patches with equal repair/patch volume in a double picture frame fixture with large unsupported to support span ratio. It is to be noted that there was no initial damage induced on to the composite laminates for the repair, rather the central region of pristine samples was machined off as per the required dimensions (as detailed in section 2) and repaired with appropriate scarf patch repair and these were subjected to 32J impact energy in a drop-weight machine.

2. Materials, Manufacturing, and Repair Design

This section details the materials involved in the manufacturing of the laminates and determination of design space for calculation of scarf angle.

2.1. Fabrication of FRP laminates

HexPly M21/37%/7581 GFRP prepregs supplied by Hexcel Ltd® were used to manufacture the composite laminates. The E-glass prepreg is an 8-harness satin (8HS) weave has 476 g/m^2 areal density with 50% fibre volume fraction and the cured ply has 0.25 mm thickness. The prepregs layered in the sequence $[+45/0/90/-45/0/+45]_s$ was vacuum debulked to remove the trapped air and to achieve a nearly void-free laminate of 3 mm nominal thickness using 12 plies. Herein, the 0^o is considered to be the prepreg warp direction of the roll and with 50% fiber volume along warp and weft directions is expected to give the in-plane quasi-isotropy. Finally, it was cured in an autoclave under 0.1 MPa vacuum (to keep the debulking for voids removal), the consolidation pressure of 0.7 MPa, and held at 180°C temperature for 120 minutes. Similarly, repair patch was manufactured with same fiber orientation and autoclave curing program as that of the parent laminate.

2.2. Design and repair of laminates

 doi:10.20944/preprints202304.0866.v1

Determination of the optimal scarf angle was adopted from our previous work as summarised by Prabhu et.al., [17], where the authors have employed same HexPly M21/37%/7581 GFRP prepreg and strong, high-temperature resistant AF3109-2K thermosetting modified epoxy scrim supported structural film adhesive (supplied by 3M) with 60MPa tensile strength and 2.8GPa Young's modulus (mode I and mode II fracture toughness measured under double cantilever beam (DCB) and end notch flexural (ENF) tests was 1.71 kJ/m^2 and 6.92 kJ/m^2, respectively). The optimal scarf angle range for three-dimensional repair of the 3 mm thick laminate was determined to be in between 2.66^o - 4.82^o. The required scarf angle to meet the design ultimate strength requirement is typically small for highly loaded composite structures. However, the use of small scarf angle results in very high stress concentration at the feathered tip and low residual strength unable to meet the design limit load (DLL). In addition to that, shallow or small scarf angles also require greater material removal from the undamaged region which can substantially increase machine time and possibility of machine induced damage.

Therefore, from the limits determined, scarf angle of 3^o was chosen. The manufactured laminates were machined using abrasive water jet to a sample size of 250 x 250 x 3 mm. To repair the damaged region, it must be completely removed and encapsulated within lower patch cut out, which dictates the shape of the upper repair region. Wang and Gunnion [14] developed a numerical study with the aim of presenting an optimum scarf shape. Their results revealed that significant savings can be made to the amount of material removal (between 26% and 76%), by adopting optimum repairs over conventionally designed repairs under in-plane loading conditions. Furthermore, for low scarf angle, their optimum scarf shape resulted to be close to a concentric ellipse with the aspect ratio being approximately equal to the biaxial stress ratio. Additional results also indicated that a hybrid square ellipse profile for high aspect ratio damage can further reduce repair size. Figure 1(a) illustrate typically seen elongated damaged profile and commensurate circular as well as rounded rectangular design. A rounded rectangular repair patch has 27.5% less volume compared to that of circular repair patch, which also translates to lower undamaged material removal during the machining process.

Preprints (www.preprints.org) | NOT PEER-REVIEWED | Posted: 25 April 2023 doi:10.20944/preprints202304.0866.v1

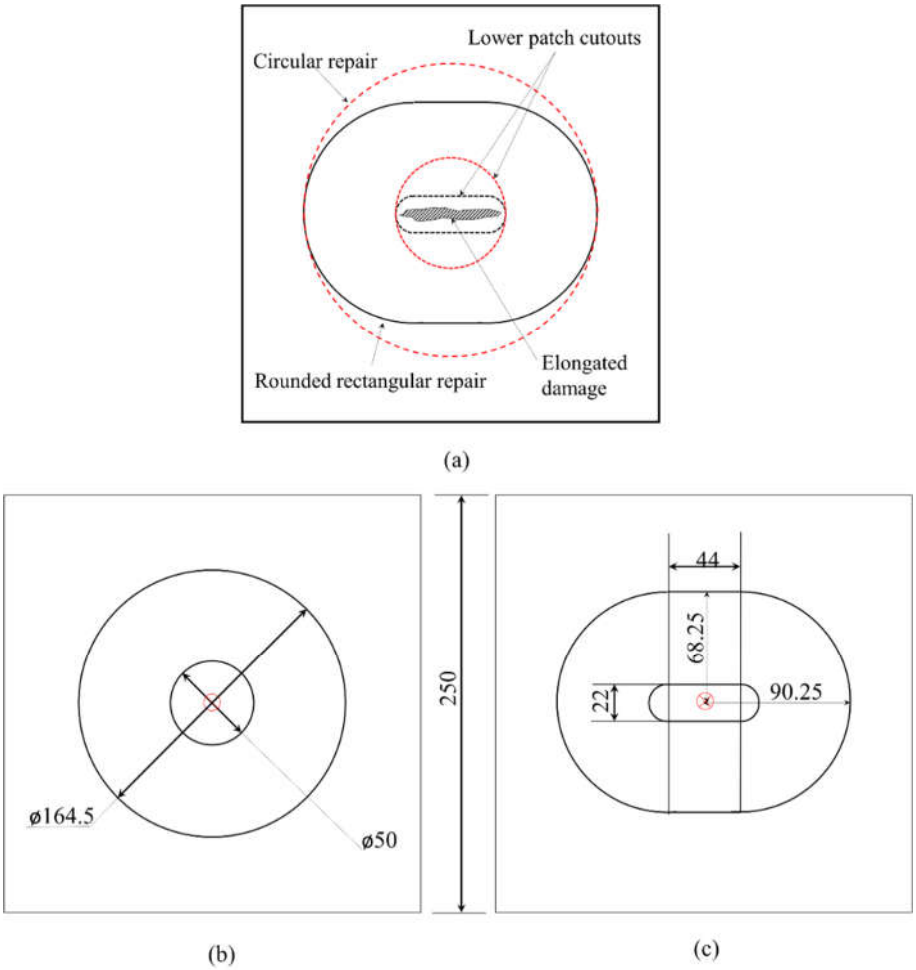

Figure 1. a) Aerial difference between circular and rounded rectangular repairs for same elongated damage profile. Patch designs for a 3° scarfed repair with similar volume of material removed in (b) circular, and (c) rounded rectangular profile (all dimensions are in mm).

Three samples tested under pristine (A, B, C), circular patch (D, E, F) and rounded rectangular patch (G, H, I) joined categories. In this study, our objective is to understand the impact performance of circular and rounded rectangular patch bonded with same volume of material removed during the joining process while machining a 3° scarf angle on a 250 x 250 x 3 mm (Figure 1(b) and 1(c)). As such there was no initial impact damage created on the neat samples, rather to simulate the circular or rounded rectangular patch bonded joints in scarf configuration, pristine samples are machined as required. The approach for scarf repair involves machining the laminates with the help of pneumatically driven step sander with jigs which facilitates the localized repair. A 7 mm 85/100 Diamond Surface Planer was chosen to sand the surface of the composite. Its high roughness index ensured there is proper mechanical anchorage as well as there is no machine induced delamination. Adherend bonding surface was dry grit blasted for 30 ± 5 s at 250 kPa with 120 μm white alumina powder, which gave a surface roughness (R_a) of 3.40 μm and water contact angle of 45°. After cleaning with deionized water, the samples were dried inside an air circulating oven for 30 min at 60 °C and degreased with acetone before layering with a single film of AF3109-2K. The overall bonding area for circular scarf and rounded rectangular scarf repaired samples were computed to be 19315.13 mm^2 and 19317.9 mm^2 respectively. To avoid film adhesive crimping during the application, the bonding zone was divided into four sectors and the adhesive film was cut to the shape of the four sectors. After application of adhesive film in the cavity the patch was assembled on it such that the fiber orientation of the patch matches with the parent laminate. The repair patch-cavity assembly were then debulked for a duration of 20 minutes before the repair After the debulking process, the

Preprints (www.preprints.org) | NOT PEER-REVIEWED | Posted: 25 April 2023 doi:10.20944/preprints202304.0866.v1

single layer adhesive film in between the adherend surfaces were cured using the Heatcon® HCS9200B dual zone hot bonder.

3. Experimental Methods

A cone shape steel impactor with a diameter of 25 mm hemispherical head shown in Figure 2(a) was used as the drop weight impactor. An accelerometer was fastened to the 3.5 kg impactor to measure the acceleration of the impactor during the testing. The experimental setup of the tool drop test is shown in Figure 2(b), the outer 12.5 mm width of specimen is clamped by hollow double picture frame such that the central 225 x 225 mm area is not supported. The impactor was allowed to slide freely inside a PVC guide tube at predetermined height. A slit was cut on the guide tube for the wires on the accelerometer to move freely with the impactor. All edges of specimen were fixed with a picture frame on a metal surface plate. A force sensor was sandwiched between surface plate and a heavy metal base to obtain the impact force. An oscilloscope was used to collect data from the force sensor and the accelerometer. A high-speed camera was placed at the same height of the panel surface to record the impact process and calculate impact velocity and rebound velocity. The initial impact velocity was estimated based on the potential energy of the impactor. The actual initial impact velocity (v_i) and rebound velocity (v_r) are obtained using the high-speed camera images. Therefore, the absorbed energy E_a is given as:

$$E_a = \frac{1}{2}m({v_i}^2 - {v_r}^2) \quad (1)$$

where m is mass of the impactor. The velocity during the impact is calculated using:

$$v(t) = v_i - \int_0^t a(t')\,dt' \quad (2)$$

where $a(t')$ is the acceleration data from the accelerometer attached to the impactor. The displacement-time history $\delta(t)$ is calculated by Newton's second law as:

$$\delta(t) = v_i t - \int_0^t \left[\int_0^{t'} a(t')\,dt'\right] dt \quad (3)$$

In the current impact experiments, the impactor drop height was set to 1.07 m, resulting an impact velocity of 4.61 m/s and loading the samples at 37 J. This is a typical high energy (beyond 25 J), these tests were conducted as part of evaluating component repair during the event of accidental tool drop during MRO procedures [4].

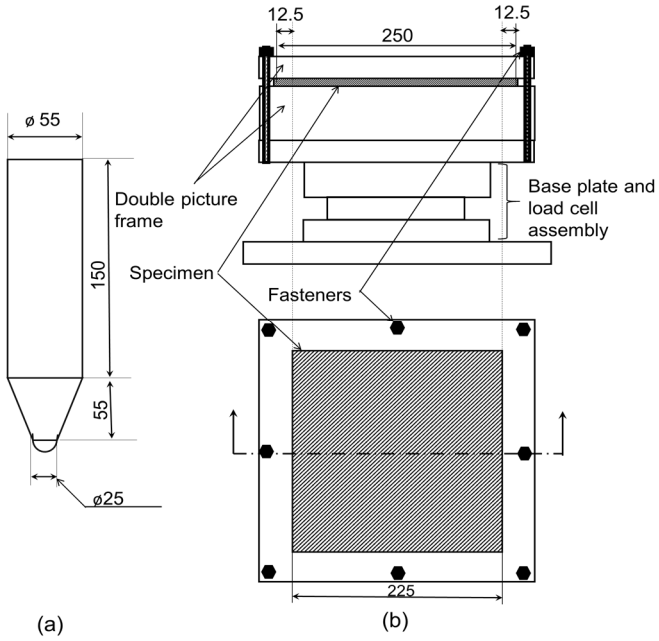

Figure 2. (a) projectile profile and (b) impact fixture setup (all dimensions are in mm).

Preprints (www.preprints.org) | NOT PEER-REVIEWED | Posted: 25 April 2023 doi:10.20944/preprints202304.0866.v1

4. Results and Discussion

The force-time history of the impacted samples is plotted in Figure 3, as the impactor impinges the test sample initially it can be observed that the load increases sharply due to Hertzian contact and has a sudden drop. The Hertzian contact force of pristine and circular repaired samples is (3.68 kN) and that of rounded rectangular repair sample is 3.87 kN which is 5.1 % higher than pristine sample. Hirai et al. [18] in their work which dealt with impact response of the woven fabric found that the incipient damage load in their tests on woven GFRP laminates was a consequence of interface failure or matrix cracking near the tension dominant side (bottom side) of the laminates and is given in terms of mode-II fracture toughness (G_{IIc}) as [19] (the predictions of threshold load value for damage initiation from this simplified model were shown to be in good agreement with experimental load values that correspond to the initial occurrence of damage [20]),

$$P^2_{cr} = \frac{8\pi^2 E t^3 G_{IIc}}{9(1-\nu^2)} \quad (4)$$

where, E (24 GPa) and υ are the flexural modulus, Poisson's ratio of the laminate, t is thickness and G_{IIC} is the mode -2 fracture toughness of the laminate (4.55 kJ/mm² [21]). Through Equation 4, it was found that the critical failure load (P_{cr}) for the GFRP laminates used was 5.1 kN. The peak force observed from the tests are listed in Table 1: pristine samples show maximum force of 8.39 kN, circular patch repair samples is at 7.72 kN and rounded rectangular ones at 7.14 kN. The oscillations within the Hertzian contact and subsequent rise of load can be attributed to impactor ringing and flexural vibration of the impacted specimen. After the Hertzian contact, the load exceeded the P_{cr} along with large oscillations to the peak observable load. Following peak load, the impactor was allowed to rebound three times till the energy completely dissipated and was able to mimic accidental tool drop in the targeted component.

Table 1 Peak force response of specimens

Specimen	Pristine sample	Circular Patch Repair			Rounded Rectangular Patch		
	A	B	C	D	E	F	G
Peak force (kN)	8.39	7.35	8.14	7.67	7.44	6.98	6.99

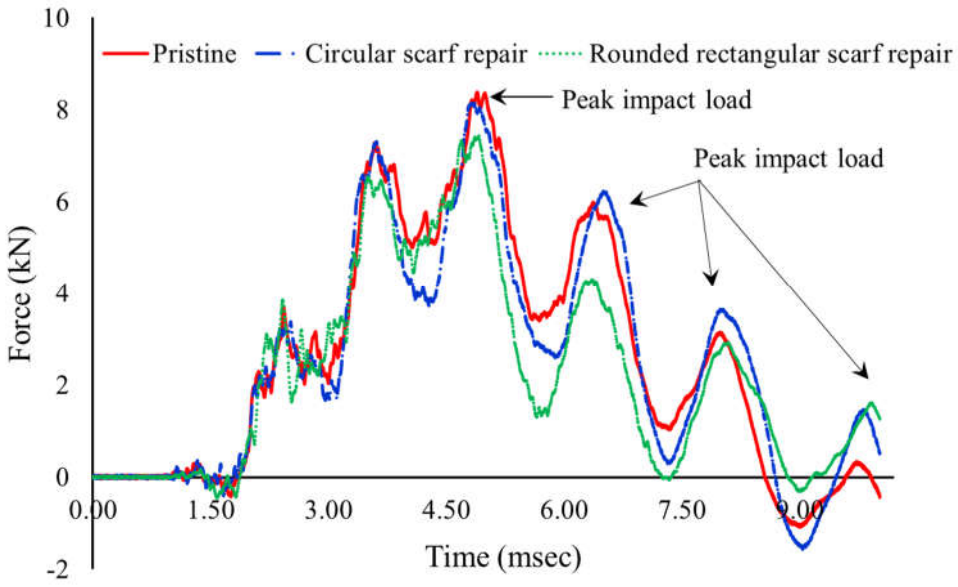

Figure 3. Force versus time response of impacted samples.

Preprints (www.preprints.org) | NOT PEER-REVIEWED | Posted: 25 April 2023 doi:10.20944/preprints202304.0866.v1

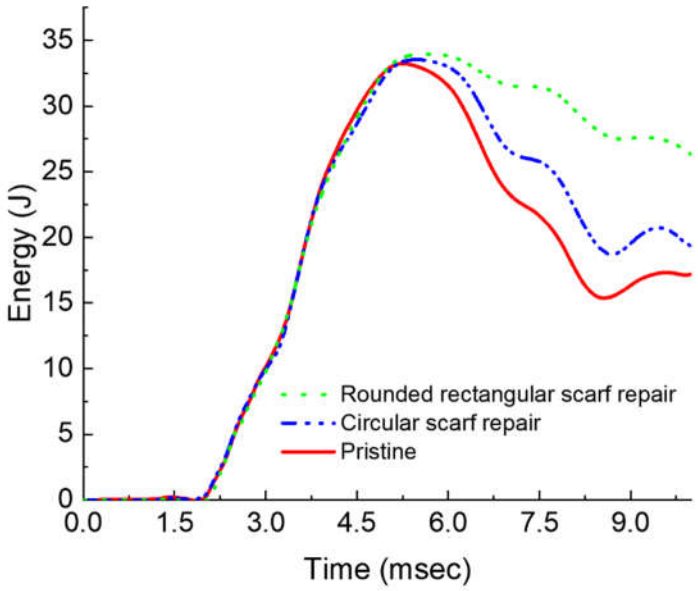

Figure 4. Energy versus time response of impacted laminates.

Typical impact energy versus time responses is depicted in Figure 4. Within experimental scatter, the peak energy absorbed by all the three samples is around 33.5 J, close to that of 37J potential energy imparted by the drop-weight. It is to be clarified that the energy plot in figure 4 has been plotted for total duration of the experiment, whereas in Figure 3 the impact event starts at ~1.5 msec and ends at about 9.5 msec with impact event duration being 8.5 msec approximately. According to the energy profile diagram (EPD) proposed by Liu [22], the closeness of impact and absorbed energy indicate the laminate failure by projectile through penetration. It can be observed that the rounded rectangular repaired sample (I) has absorbed 52% energy more compared to pristine and 36% more compared circular scarf repaired laminates post peak energy at the point of impact. High energy absorption by the rounded rectangular scarf repair can be directly correlated to its damage area (Figure 5), which will be discussed in section 4.1. Similarly, the energy absorbed by the circular scarf repaired samples post peak energy at the point of impact is greater than pristine and its damage area (Figure 5) is also larger compared to pristine.

4.1. Failure Analysis

Following impact tests, the samples were retrieved for failure examination, it was observed that all the samples impacted at 37 J had a damage region which included a centrally depressed region/permanent indentation, matrix cracking, localized delamination areas, and fiber fracture. Figure 5 shows visually observed impact damages on the three tested specimens. Prior to taking images (with Nikon Z camera with NIKKOR Z 35mm f/1.8 S lens on a manual focus setting) the samples were coated with black ink and wiped such that the intricate cracks are filled with ink and the samples were dried in a convection oven at 85°C. The samples placed in the picture frame with high intensity white light behind the sample. The translucency of the samples enabled to discern discontinuous fibers as well as matrix and black ink helped in accentuating the difference more lucidly. The damage region was cropped with greyscale inversion to discern the surficial cracks from the undamaged surface.

The damage region of the pristine and circular scarf repair specimens are relatively symmetrical quatrefoil and trefoil shape, respectively, whereas rounded rectangular scarf repair specimens is asymmetrical with predominant delamination towards the major axis of the rounded rectangle. The damage area was calculated in such a way that the point of impact was considered as center of damage and the crack that propagated to the maximum length from the center is the radius of the circle of damage. The area of circle is what gives us the damage area. The reason for circle being considered as the damage area is one has to machine this area for repair purposes. So, the damage

Preprints (www.preprints.org) | NOT PEER-REVIEWED | Posted: 25 April 2023 doi:10.20944/preprints202304.0866.v1

area is computed as a circular region whose radius is the furthest point of the delamination region from the impact point. The damage size in circular and rounded rectangular repairs are on an average greater by 9.91% and 434.23%, when compared to the pristine sample.

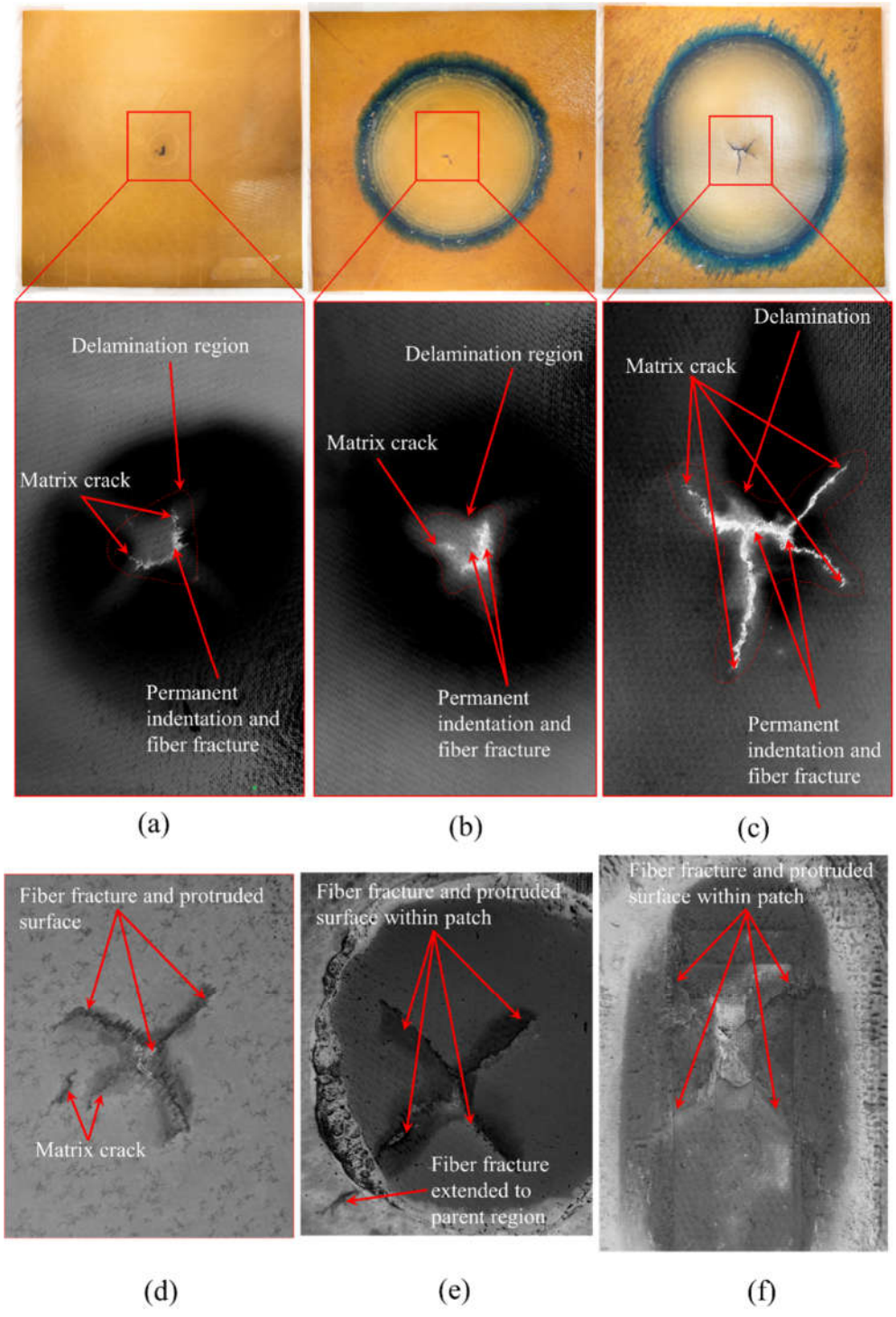

Figure 5. Visually observed (top view, bottom view) impact damages of: (a, d) pristine laminate; (b, e) circular scarf repaired laminate and (c, f) rounded rectangular scarf repaired laminate.

The damage areas are approximately 181.63 mm², 199.64 mm², 970.33 mm², respectively for pristine, circular, and rounded repair specimens. It is also noticed that the size of damage is being influenced by the patch symmetry, as depicted in Figure 1, despite circular and rounded rectangular scarf repaired samples having similar bonding area 19315.13 mm² and 19317.9 mm² respectively. The

Preprints (www.preprints.org) | NOT PEER-REVIEWED | Posted: 25 April 2023 doi:10.20944/preprints202304.0866.v1

damages witnessed in rounded rectangular scarf repaired laminates are oriented towards the major axis of the patch, whereas the damage propagation in minor axis is limited within the bottom cut out.

Tested samples were further inspected with the help of Nikon XTH 225 ST computed tomography (CT), where the raw images were reconstructed by segmenting the volume. From the scanned images, voxels (volumetric elements) were adjusted by changing the isosurface setting to visualize the impact damages and fibre yarn. Figure 6 illustrates the damage area relative to the damage size in the top ply across various plies. Figure 7 illustrates the damage propagation across various plies in through thickness. It can be seen that the pristine and circular scarf patch repaired laminate (Figures 7a and 7b) had demonstrated similar pine tree pattern [23], whereas in rounded rectangular repaired laminate (Figure 7(c)) had cylindrical pattern. These results can also be translated degradation of bending stiffness with change in the sample configuration [24] i.e. pristine sample has highest bending stiffness amongst tested samples followed by circular and rounded rectangular repaired scarf patch laminates.

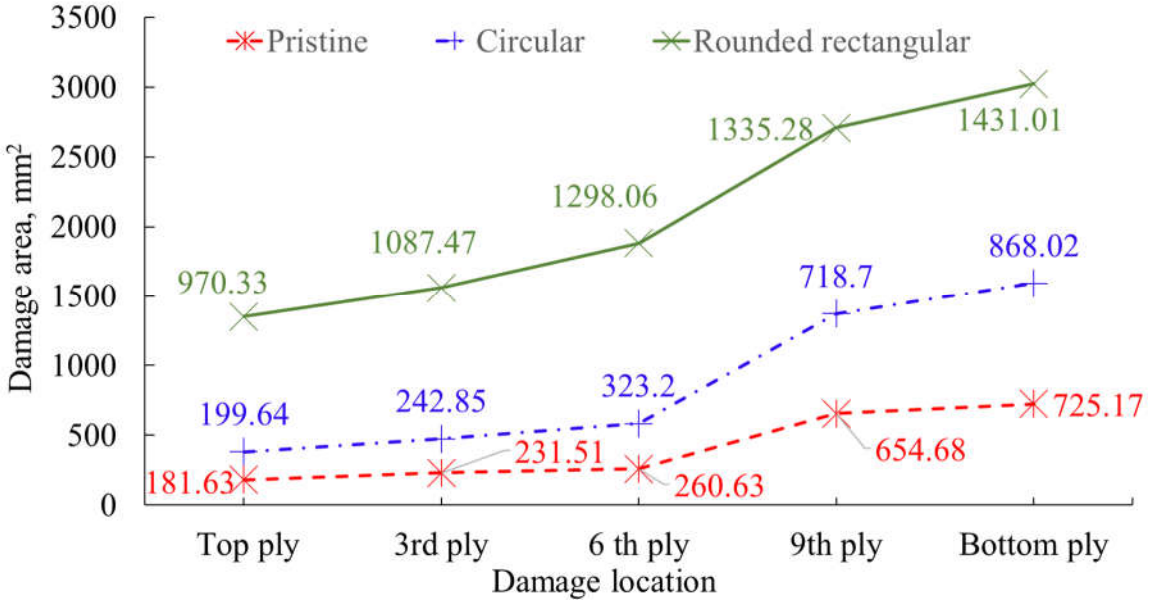

Figure 6. Damage area for different plies for tested configurations.

Preprints (www.preprints.org) | NOT PEER-REVIEWED | Posted: 25 April 2023 doi:10.20944/preprints202304.0866.v1

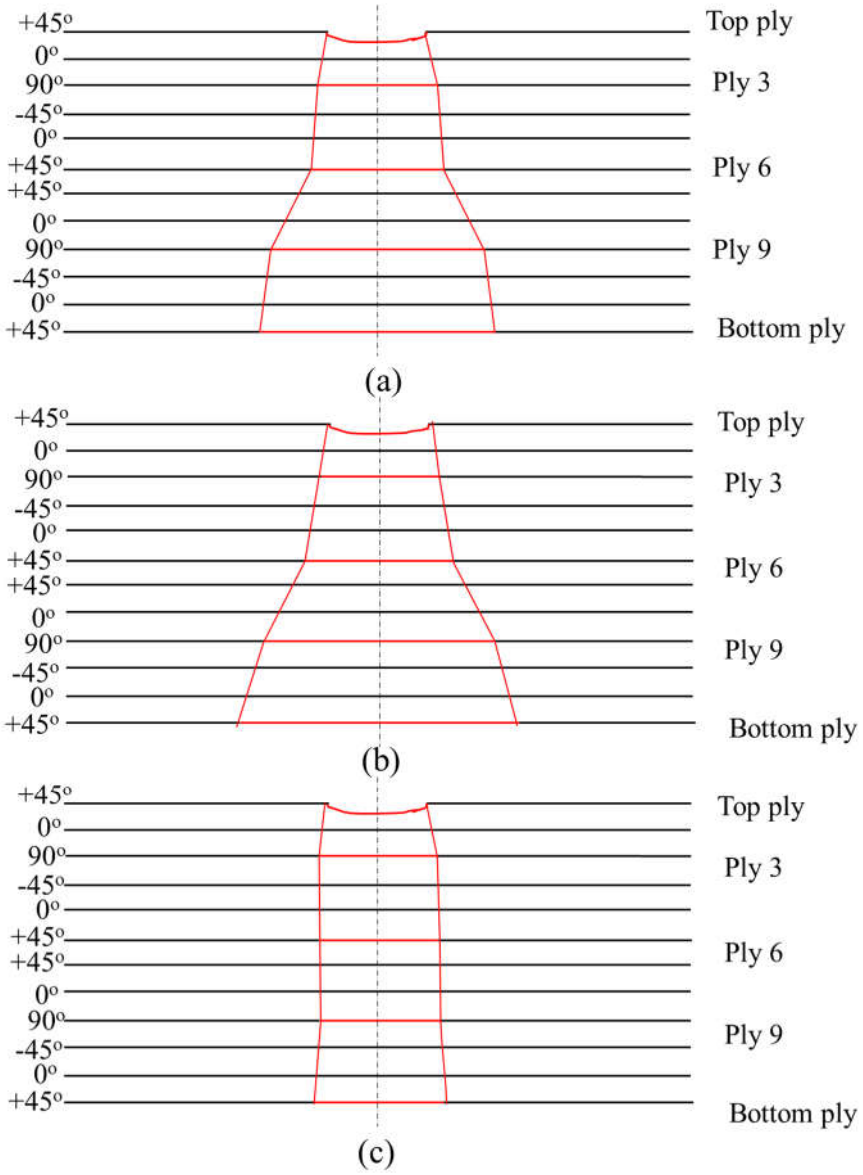

Figure 7. Cross sectional damage profile with respect to the size of the top ply damage area of (a) pristine laminate; (b) circular scarf repaired laminate and (c) rounded rectangular scarf repaired laminate.

Figures 8 and 9 shows CT scan image slices in the top, third, sixth, ninth and bottom plies, and depicts the cross-sectional view of the damaged laminates. We observe that the damage size from top to bottom ply gradually increases for both pristine and circular patch repaired laminate, whereas it is almost constant for the rounded rectangular patch laminate. In both pristine and circular repaired patch laminate the evidence of fibre breakage can be witnessed in the plies beneath ply 6 (Figure 9(a)) and ply 5 (Figure 9(b)) respectively, in the case of rounded rectangular patch repaired laminate the onset of fibre failure is witnessed from ply 3 onwards (Figure 9(c)). Figure 8 reveal that all three tested sample undergo permanent indentation at the point of impact. The permanent indentation in rounded rectangular scarf repaired laminate is most obvious due to maximum roving failure at the bottom side of the laminate enabling greater projectile penetration. It is also noted that the strong aerospace grade structural adhesive AF3109-2k used in this work, was able to eliminate cohesive failure of the adhesive as its mode II fracture toughness of 6.92 kJ/mm^2 is 1.5 times higher than that of laminate material, and the surface preparation able to resist adhesive failure, under 32J impact energy.

Preprints (www.preprints.org) | NOT PEER-REVIEWED | Posted: 25 April 2023 doi:10.20944/preprints202304.0866.v1

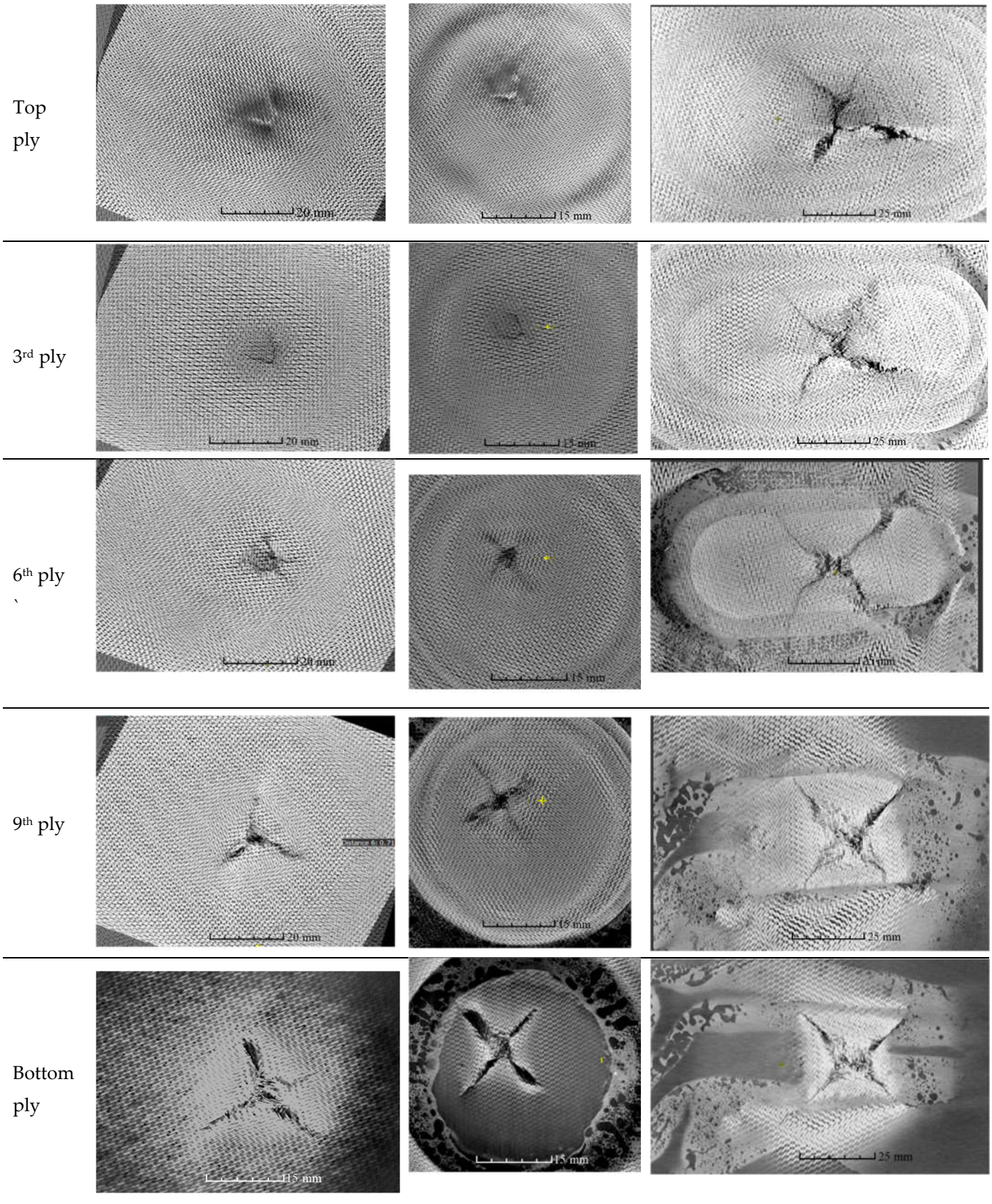

Figure 8 CT scan images for various plies for (a) pristine, (b) circular repair and (c) rounded rectangular repair.

Preprints (www.preprints.org) | NOT PEER-REVIEWED | Posted: 25 April 2023 doi:10.20944/preprints202304.0866.v1

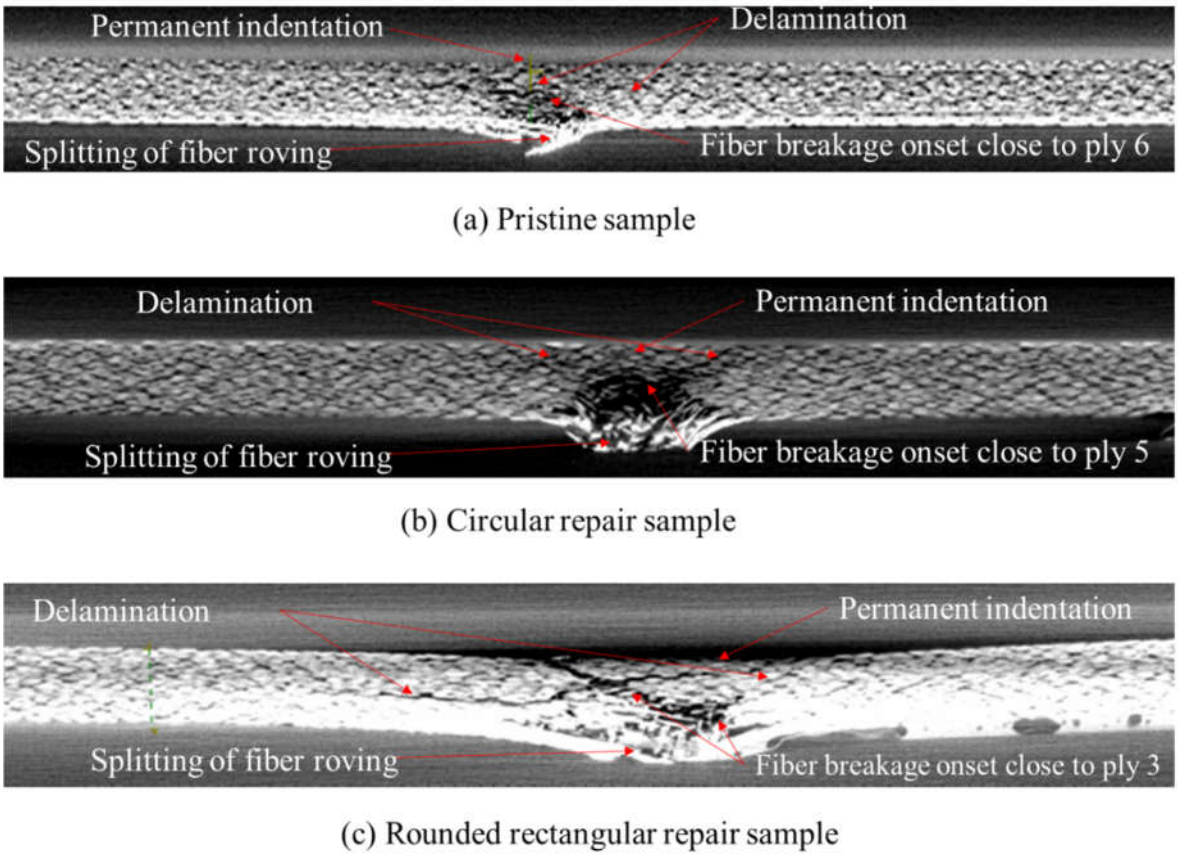

Figure 9 Cross sectional view of (a) pristine, (b) circular and (c) rounded rectangular repair.

5. Conclusion

This work was carried out to further explore and experimentally validate alternative scarf cut out shape options against conventional circular scarf cut outs for localized repairs which have greater material removal and proportionate machining time penalties. An optimal scarf cut out shape which sufficiently encompasses the damaged region would reduce the down time of the damaged component along with optimal usage of repair materials, thereby making this a sustainable engineering approach. Critical assessment of current scarf repair design methodologies has revealed that significant savings can be made to the amount of material removal when adopting rounded rectangular repair over conventionally designed circular scarf repaired laminate. Through impact testing it was revealed that the repairs conducted with similar material volume removed demonstrated different severity of failure modes governed by the symmetricity along major and minor axes. Impact resistance of rounded rectangular scarf repair laminate was only 12.9 % lower compared to the pristine whereas circular scarf repaired laminate was only 3 % lower compared to the pristine. From the CT scan and visual inspection, it was evident that the rounded rectangular scarf repaired laminate incurred maximum damage compared to the circular repair scarf and pristine laminates, though all three had absorbed the similar energy during impact event. It was observed that the energy absorbed by the samples during the impact event is close to the impact energy of the projectile, which was clear as all the samples demonstrated fiber failure and permanent indentation. The rounded rectangular repaired laminates demonstrated maximum permanent indentation, whereas circular scarf repaired, and pristine laminates had least permanent indentation. This research concludes that a localized repair with rounded rectangular scarf repair has small depreciation in peak impact loading but with a greater damage area can still be viable repair option

considering the down time and material savings. The strong and tough structural film adhesive AF3109-2K was able to resist the adhesive failure for both the cases.

Acknowledgement: This work was financially supported from the National Research Foundation (NRF) of Singapore under Corporate Laboratories @ Universities Scheme (ARMS 1.3 project). Authors thank Mr Elton Tan of NTU and Prof. TE Tay of National University of Singapore for the experimental assistance.

Declaration of interests: The authors declare that they have no known competing financial interests or personal relationships that could have appeared to influence the work reported in this paper.

Data Availability Statement: All data generated or analysed during this study were included in this published article and raw data will be made available upon request.

Author contributions: The work was part of hybrid composites or sandwich repair project under the supervision of Sridhar Idapalapati as Principal Investigator. Sridharan Vijay Shankar conceptualized designs for the repair, developed fixtures, analyzed data at the component level. Sridharan Vijay Shankar drafted the initial manuscript, which was revised by Sridhar Idapalapati.

References

1. Alves, M., C. Chaves, and R.S. Birch. *Impact on aircraft*. in *Proceedings of the XVII Brazilian Congress of Mechanical Engineering*. 2003.
2. Trias, D. and P. Maimí, *Micromechanical Analysis of Mode I Crack Growth in Carbon Fibre Reinforced Polymers*, in *Damage and Fracture of Composite Materials and Structures*. 2012, Springer. p. 17-26.
3. Panettieri, E.; Fanteria, D.; Montemurro, M. and Froustey, C., *Low-velocity impact tests on carbon/epoxy composite laminates: a benchmark study*. Composites Part B: Engineering, 2016. **107**: p. 9-21.
4. Aktaş, M., et al., *An experimental investigation of the impact response of composite laminates.* Composite Structures, 2009. **87**(4): p. 307-313.
5. Koloor, S., et al., *Evolution characteristics of delamination damage in CFRP composites under transverse loading*, in *Damage and Fracture of Composite Materials and Structures*. 2012, Springer. p. 45-59.
6. Hall, Z., et al., *The effectiveness of patch repairs to restore the impact properties of carbon-fibre reinforced-plastic composites.* Engineering Fracture Mechanics, 2022. **270**: p. 108570.
7. Shufeng, L., et al., *Study on impact performances of scarf-repaired carbon fiber reinforced polymer laminates.* Journal of reinforced plastics and composites, 2015. **34**(1): p. 60-71.
8. Ramji, M.; Srilakshmi, R. and Prakash, M.B., *Towards optimization of patch shape on the performance of bonded composite repair using FEM.* Composites Part B: Engineering, 2013. **45**(1): p. 710-720.
9. Duong, C.N. and C.H. Wang, *Composite repair: theory and design*. 2010: Elsevier.
10. Ahn, S.-H. and G.S. Springer, *Repair of composite laminates-I: test results.* Journal of Composite Materials, 1998. **32**(11): p. 1036-1074.
11. Cheng, P., Gong, X.J; Aivazzadeh, S. and Xiao, X., *Experimental observation of tensile behavior of patch repaired composites.* Polymer testing, 2014. **34**: p. 146-154.
12. Bhatia, G.S., Andrew, J.J.; Balaganesan, G. and Arockiarajan, A., *The role of patch-parent configurations on the tensile response of patch repaired carbon/epoxy laminates.* Polymer Testing, 2018. **70**: p. 413-425.
13. Hoshi, H., Nakano, K. and Iwahori, Y. *Study on repair of CFRP laminates for aircraft structures*. in *Proceedings 16th international conference on composite materials*. 2007.
14. Wang, C.H. and Gunnion, A.J., *Optimum shapes of scarf repairs.* Composites Part A: Applied Science and Manufacturing, 2009. **40**(9): p. 1407-1418.

 doi:10.20944/preprints202304.0866.v1

15. Tie, Y., et al., *An insight into the low-velocity impact behavior of patch-repaired CFRP laminates using numerical and experimental approaches.* Composite Structures, 2018. **190**: p. 179-188.
16. Kashfuddoja, M. and Ramji, M. *Design of optimum patch shape and size for bonded repair on damaged Carbon fibre reinforced polymer panels.* Materials & Design (1980-2015), 2014. **54**: p. 174-183.
17. Prabhu, G., Katakam, V., Sridharan, V.S. and Idapalapati, S., *Uniaxial tensile failure of multi-core asymmetric sandwich composite structures with bonded repair.* Composite Structures, 2019: p. 111025.
18. Hirai, Y; Hamada, H. and Kim, J.-K. *Impact response of woven glass-fabric composites—I.: Effect of fibre surface treatment.* Composites Science and Technology, 1998. **58**(1): p. 91-104.
19. Davies, G. and Zhang, X., *Impact damage prediction in carbon composite structures.* International Journal of Impact Engineering, 1995. **16**(1): p. 149-170.
20. Gliszczynski, A., Kubiak, T. and Wawer, K., *Barely visible impact damages of GFRP laminate profiles–An experimental study.* Composites Part B: Engineering, 2019. **158**: p. 10-17.
21. Schwab, M. and Pettermann, H., *Modelling and simulation of damage and failure in large composite components subjected to impact loads.* Composite Structures, 2016. **158**: p. 208-216.
22. Liu, D., *Characterization of impact properties and damage process of glass/epoxy composite laminates.* Journal of Composite Materials, 2004. **38**(16): p. 1425-1442.
23. Minak, G., Fotouhi, M. and Ahmadi, M., *Low-velocity impact on laminates*, in *Dynamic Deformation, Damage and Fracture in Composite Materials and Structures*. 2016, Elsevier. p. 147-165.
24. Liu, D., *Impact-induced delamination—a view of bending stiffness mismatching.* Journal of composite materials, 1988. **22**(7): p. 674-692.